Electron Transfer-Induced *cis*−*trans* Isomerization of $[Mn(CN)(CO)_2\{P(OPh)_3\}(Ph_2PCH_2PPh_2)]$: Solution and Solid State Voltammetric Studies

Conor F. Hogan,[†] Alan M. Bond,*[,†] Aaron K. Neufeld,[‡] Neil G. Connelly,*[,§] and Estefania Llamas-Rey[§]

School of Chemistry, Monash University, Clayton, Victoria 3800 Australia, CSIRO—Manufacturing and Infrastructure Technology, P.O. Box 56, Graham Road, Highett VIC 3190, Australia, and School of Chemistry, University of Bristol, Bristol BS8 ITS U.K.

Received: November 22, 2002

Fast scan rate cyclic voltammetry has been used to elucidate the heterogeneous and homogeneous aspects of the redox chemistry of *cis*- and *trans*-$[Mn(CN)(CO)_2\{P(OPh)_3\}(Ph_2PCH_2PPh_2)]$. The *cis* species, on oxidation, isomerizes to the *trans* conformation, and the various processes can be understood as components of a square reaction scheme. In solution phase, the homogeneous rate constant for isomeric conversion is found to be independent of solvent and concentration, with a value of 38 s^{-1} obtained by comparison with digitally simulated responses. The heterogeneous rate constants for the cis^0/cis^+ and $trans^0/trans^+$ couples in acetonitrile have values of 0.06 and 0.065 cm s^{-1} respectively. The *cis* or *trans* complex was readily immobilized on an electrode surface, either by mechanical attachment or by precipitation from solution. However, electrolysis in the solid state was strongly dependent on the identity of the supporting electrolyte anion. This dependence is similar to the Hofmeister series of anions with large, hydrophobic ions favored in the charge-neutralization process. The addition of acetonitrile to the aqueous electrolyte solution dramatically increases the magnitude of the voltammetric peak currents but only in the presence of these ions. The effect is reversible, and other organic solvents have a similar effect. Infrared measurements conducted on the solid immobilized on glassy carbon before and after electrolysis clearly demonstrate the occurrence of the *cis*−*trans* isomerization in the solid state. The isomerization rate is considerably slower in the solid matrix relative to that in solution phase because of the restriction of free space; voltammetric measurements conducted on the solid *cis* complex immobilized on an electrode surface reveal a rate constant of 2 s^{-1}. The solvent independence of the isomerization rate in solution phase and the fact that the reaction is observed with an appreciable rate in the solid state suggest that the conformational change occurs via a nondissociative twist mechanism. Morphological changes accompanying the solid-state redox electrochemistry, observed with both thin and thick coatings of microparticles, were evaluated by electron scanning microscopy and revealed the formation of needlelike crystals on the electrode surface during the course of potential cycling experiments.

Introduction

Structural changes induced by electron transfer are a matter of continuing interest in chemistry. For example, knowledge of how metal complexes respond structurally to changes in their redox state is crucial to understanding the mechanisms of metal charge-transfer reactions and impacts areas such as photoelectrochemistry,[1,2] organometallic catalysis,[3] molecular electronics,[4] supramolecular chemistry,[5] and biologically important systems.[6]

In cases where the intramolecular reaction occurs on a sufficiently short time scale, the structural rearrangement between reactant and product is considered to be concerted with the actual electron transfer and results in slow heterogeneous kinetics, as is the case, for example, with changes in the bonding mode observed on oxidation of some molybdenum complexes.[7] However, when the structural change is relatively slow, it can be regarded as being temporally distinct from the charge-transfer process, and the situation is most conveniently described in terms of an EC mechanism or, if all steps are interconnected, as a square scheme.[8] In these instances, kinetic parameters associated with the constituent reactions can then often be deduced using conventional voltammetric techniques. This has been achieved in a number of cases for species in the solution phase.[9−11] However, evaluation of the kinetics of these processes in solid state/adsorbed systems is rare,[12,13] and in particular, the issue of comparison between solution and solid phase[14] remains largely unexplored.

Recently, the development of techniques for the mechanical attachment of solid microparticles to electrodes has enabled electrochemical studies to be undertaken, in principle at least, on any redox-active compound in the solid state.[15] The study of the electrochemistry of solid compounds in this manner is of great importance both for the development of a fundamental understanding of interfacial reactions and for applied science. Solid-state electrochemistry has been used to study processes such as nucleation and growth phenomena, electrocrystallization, and charge transport through solid materials.[16] Isomerization within microcrystals of a chromium carbonyl derivative has been reported,[17] and lattice reconstructions have been observed on reduction of solid films of a Prussian blue analogue.[18,19]

* To whom correspondence should be addressed. E-mail: alan.bond@sci.monash.edu.au. E-mail: neil.connelly@bristol.ac.uk.
[†] Monash University.
[‡] CSIRO—Manufacturing and Infrastructure Technology.
[§] University of Bristol.

10.1021/jp027529y CCC: $25.00
Published on Web 02/07/2003

However, homogeneous kinetic processes have not been studied in detail in solid matrices of this type.

Electrochemical studies on manganese derivatives in the past have led to the discovery of oxidatively induced isomerization[20] and have provided routes to otherwise inaccessible geometric isomers.[21] In this contribution, we have systematically evaluated the electrochemical properties associated with the oxidation of the *cis* and *trans* isomers of the 18-electron octahedral-type complex $[Mn(CN)(CO)_2\{P(OPh)_3\}(Ph_2PCH_2PPh_2)]$ in solution phase as well as immobilized on an electrode surface in the solid state and have quantitatively probed the kinetics of the *cis*−*trans* isomerization in both phases using rapid scan voltammetry.

Experimental Section

Materials. *cis*-$[Mn(CN)(CO)_2\{P(OPh)_3\}(Ph_2PCH_2PPh_2)]$ (Mn-*cis*) and *trans*-$[Mn(CN)(CO)_2\{P(OPh)_3\}(Ph_2PCH_2PPh_2)]$ (Mn-*trans*) were prepared as described elsewhere.[22,23] Analytical reagent grade acetonitrile and dichloromethane (Aldrich) were stored over molecular sieves prior to use, and the electrolyte $[Bu_4N][PF_6]$ (GFS) was recrystallized twice from ethanol/water. Other electrolytes were of analytical grade and were used as supplied by the manufacturer (Aldrich). Aqueous solutions were prepared using deionized water (18 MΩ cm^{-1}). All solutions were deoxygenated using nitrogen for between 10 and 20 min prior to undertaking electrochemical experiments. All measurements were carried out at ambient temperature (20 ± 2 °C).

Apparatus. Morphological studies of solid layers on a 3-mm-diameter glassy carbon (BAS) electrode surface were performed using a Philips XL30 field emission scanning electron microscope (SEM) using both secondary (SE) and backscatter (BSE) imaging modes. Elements present in the solid were determined by using the Oxford Link EDAX data analysis system. The electrode surface was thoroughly rinsed with deionized water and exposed to a steady stream of nitrogen for 3 to 5 min prior to measurement to ensure the removal of electrolyte and dry conditions.

Infrared spectroscopy was conducted on the solid immobilized on a 3-mm-diameter glassy carbon electrode using a Bruker Equinox 55 spectrometer and an IR Scope II infrared microscope with an inverted Praying Mantis diffuse reflectance optical accessory. The electrode was mounted in a collar for downward positioning, ensuring that the surface of the electrode was in the focal plane of the incident infrared beam. The attached solid was rinsed and dried as described for the SEM studies prior to each measurement.

Voltammetric measurements were carried out with an Autolab PGSTAT100 (ECO-Chemie, Utrecht, Netherlands). For high scan rates (10−600 V s^{-1}), the instrument was used in the fast scan mode, making use of a high-resolution AD converter. A conventional three-electrode assembly was used: the working electrode consisted of a 3-mm-diameter glassy carbon disk shrouded in Teflon (CH instruments) or a 25-μm-diameter Pt microelectrode shrouded in glass, and a 1-cm^2 Pt gauze was used as the auxiliary electrode. The reference electrode was Ag/AgCl (3M KCl). For experiments conducted in organic solvent media, the reference electrode was separated from the test solution by a salt bridge. The formal potential ($E_f{}^0$) of the ferrocene/ferrocenium couple was 0.450 V versus Ag/AgCl in CH_3CN and 0.445 V versus Ag/AgCl in CH_2Cl_2 using 0.1 M $[Bu_4N][PF_6]$ as the supporting electrolyte. IUPAC conventions are used for the presentation of all voltammograms. Digital simulations of cyclic voltammetric responses were carried out using DigiSim software (version 3.03).

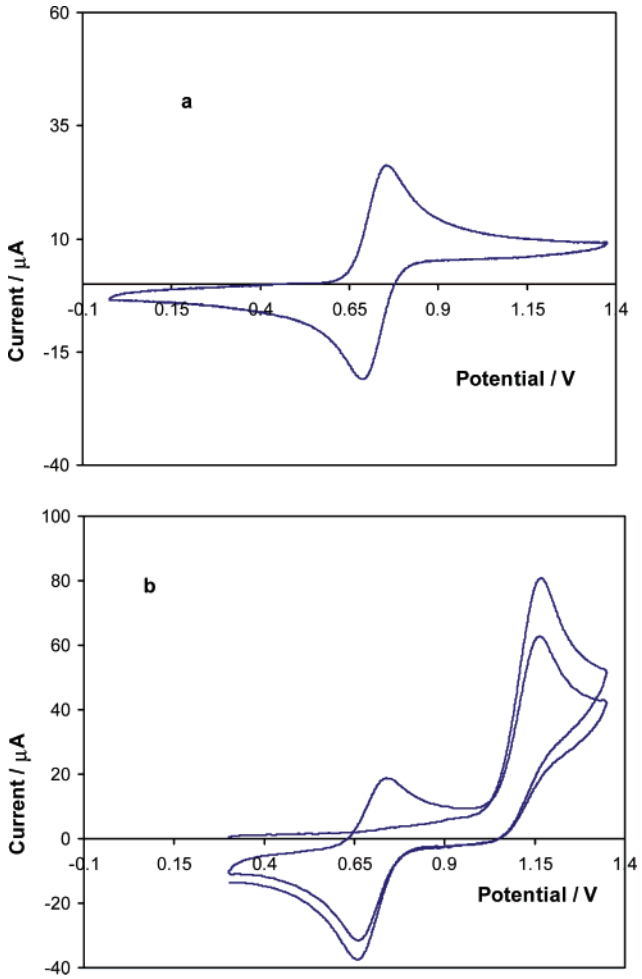

Figure 1. Cyclic voltammograms obtained at 20 °C using a scan rate of 200 mV s^{-1} with a 3-mm-diameter glassy carbon electrode for the oxidation of (a) 1.1 mM *trans*-$[Mn(CN)(CO)_2\{P(OPh)_3\}(Ph_2PCH_2PPh_2)]$ and (b) 3 mM *cis*-$[Mn(CN)(CO)_2\{P(OPh)_3\}(Ph_2PCH_2PPh_2)]$ dissolved in acetonitrile (0.1 M $[Bu_4N][PF_6]$).

Results and Discussion

***trans*-$[Mn(CN)(CO)_2\{P(OPh)_3\}(Ph_2PCH_2PPh_2)]$. Solution-Phase Electrochemistry.** Figure 1a shows the cyclic voltammetric response at a 3-mm-diameter glassy carbon electrode for a 3 mM solution of the *trans* manganese complex dissolved in acetonitrile containing 0.1 M $[Bu_4N][PF_6]$. The voltammogram displays a single reversible one-electron redox couple with a reversible potential of 0.720 V versus Ag/AgCl (average of the reduction and oxidation peak potentials) corresponding to the process Mn-$trans_{(solution)} \rightleftharpoons$ Mn-$trans^+_{(solution)} + e^-$. The value of the diffusion coefficient (D) obtained from the slope of plots of I_p versus the square root of the scan rate using the Randles−Sevčik equation under slow scan-rate conditions was (7.2 ± 0.9) × 10^{-6} cm^2 s^{-1}.

The value of the heterogeneous charge-transfer rate constant $k°$ was estimated initially in acetonitrile using the method developed by Nicholson.[24] Values of ΔE_p (difference in peak potentials) were analyzed at various scan rates ranging from 0.4 to 425.0 V s^{-1} using a 25-μm-diameter platinum microelectrode in a solution that contained 1.1 mM of the manganese complex. The contribution of uncompensated resistance on ΔE_p can readily be shown to be less than 1 mV for the highest scan rate in this study. The rate constant was determined using the following equation:

$$k° = \psi\left[\pi D_O \nu \left(\frac{nF}{RT}\right)\right]^{1/2} (D_O/D_R)^{\alpha/2} \qquad (1)$$

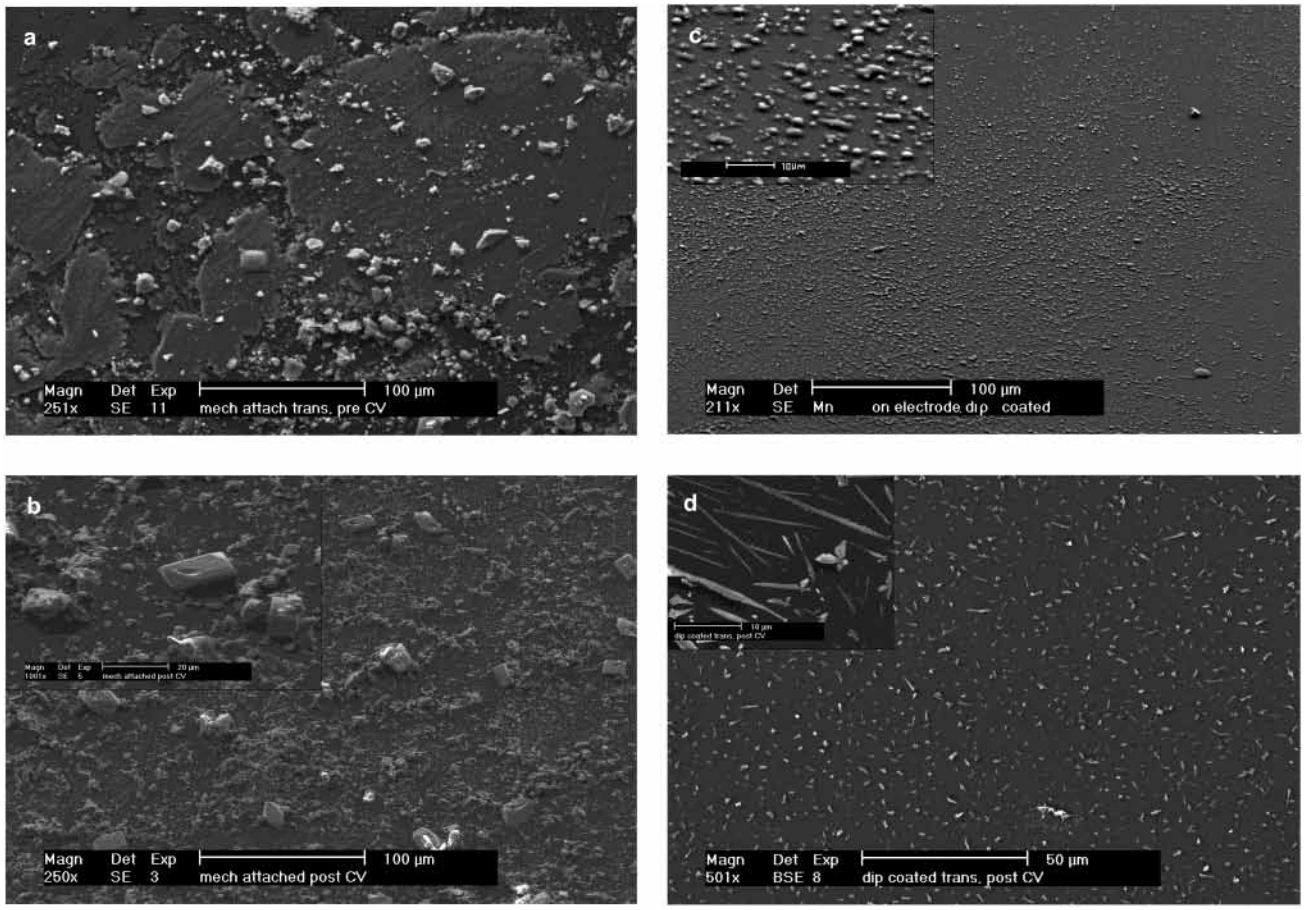

Figure 2. SEM images of *trans*-[Mn(CN)(CO)$_2${P(OPh)$_3$}(Ph$_2$PCH$_2$PPh$_2$)]. Solid mechanically attached to glassy carbon (a) before and (b) after potential cycling. (c, d) Complex immobilized by precipitation on the electrode surface (a) before and (b) after potential cycling. Twenty cycles were used over the potential range of 0.45 to 1.05 V vs Ag/AgCl in 0.1 M $LiClO_4$ aqueous electrolyte solution containing 10% CH_3CN.

TABLE 1: Summary of Electrochemical Data Obtained from a Cyclic Voltammetric Study of *cis*- and *trans*-[Mn(CN)(CO)$_2${P(OPh)$_3$}(Ph$_2$PCH$_2$PPh$_2$)] at a 3-mm Diameter Glassy Carbon Electrode in the Solution Phase at 20 °C[a]

	CH_3CN			CH_2Cl_2	
	E^0_f/V[b]	D/cm^2 s^{-1}	$k°$/cm s^{-1}	E^0_f/V[b]	D/cm^2 s^{-1}
Mn-*trans*	0.720	7.2×10^{-6}	0.065 ± 0.008	0.640	6.0×10^{-6}
Mn-*cis*	1.170	7.2×10^{-6}	0.060 ± 0.010	1.135	6.0×10^{-6}

[a] The supporting electrolyte was 0.1 M [Bu$_4$N][PF$_6$] [b] Potentials quoted relative to Ag/AgCl (3M KCl). The formal potential of the ferrocene/ferrocenium couple measured in situ was 0.450 V in CH_3CN and 0.445 V vs Ag/AgCl in CH_2Cl_2.

where D_O and D_R are the diffusion coefficients of the oxidized and reduced species, respectively, ν is the scan rate, and α is the transfer coefficient. Using a working curve that relates ΔE_p to the kinetic parameter ψ and assuming that $\alpha = 0.5$ and $D_O = D_R = (7.2 \pm 0.9) \times 10^{-6}$ cm^2 s^{-1}, the value of $k°$ was determined to be 0.065 ± 0.008 cm s^{-1} at 20 °C. Simulated voltammograms over a wide range of conditions showed an equally good fit to experimental data. Solution-phase data obtained in acetonitrile and dichloromethane are summarized in Table 1. This quantitative study is consistent with the initial report on the voltammetry of the *trans* isomer.[22]

Solid-State Electrochemistry. For solid-state voltammetric experiments, two methods were used to transfer the solid onto the working electrode. In the first, a small amount of the solid was transferred to a piece of weighing paper over which the electrode was rubbed, thus causing the solid to adhere to the surface. Figure 2a shows an SEM image of a glassy carbon electrode that has been modified in this manner with solid *trans*-[Mn(CN)(CO)$_2${P(OPh)$_3$}(Ph$_2$PCH$_2$PPh$_2$)] before exposure to electrolyte solution. As can be seen from the image, the solid adheres to the electrode in an irregular manner with a range of particle sizes present and large areas of the surface caked with solid where the compound has been compressed into a layered format. EDAX spectra taken from localized portions of the electrode surface confirm that these caked areas contain significantly larger quantities of Mn and P than adjacent areas where the electrode surface is visible. Figure 2b shows the same electrode after the potential has been cycled from 0.45 to 1.05 V versus Ag/AgCl in 0.1 M $LiClO_4$ electrolyte solution containing 10% CH_3CN for 2 min. The layer structure is altered significantly as a result of potential cycling, and a redistribution of solid occurs with the solid becoming more evenly distributed over the surface in the form of microcrystals, and more of the underlying substrate is exposed.

In the second approach to immobilization of the solid, the electrode was immersed in a 5 mM solution of *cis*- or *trans*-[Mn(CN)(CO)$_2${P(OPh)$_3$}(Ph$_2$PCH$_2$PPh$_2$)] dissolved in acetone, whereupon it was removed and immediately rinsed with deionized water, causing the solid to precipitate rapidly on the electrode. Figure 2c shows an SEM image of the electrode surface following this surface precipitation procedure, using the *trans* isomer, before exposure to electrolyte solution. The solid is far more evenly distributed over the surface than in the case shown in Figure 2a or b, and as can be seen from the inset, it seems to have deposited on the surface as an array of closely spaced particles ranging in size from 1 to 2 μm. After cycling

the potential over the range of 0.45 to 1.05 V versus Ag/AgCl in 0.1 M $LiClO_4$ solution for a period of 2 min, the physical nature of the immobilized layer is again altered dramatically. As shown in Figure 2d, small needlelike crystals, 3−15 μm long and <1 μm in width, are evenly distributed over the entire surface. The inset to Figure 2d shows an expanded view of some of these crystals. In many cases, smaller crystals have apparently grown perpendicularly from the base of a larger crystal whereas in other instances three or four crystals have grown from a single point. These observations may be a consequence of nucleation and growth phenomena initiated by voltammetric redox cycling. EDAX spectra were taken in situ for each of the SEMs shown in Figure 2, which confirmed that the crystals contained manganese and that no chlorine was present, thus ruling out the possibility of the electrode surface being contaminated with traces of supporting electrolyte.

The mechanical attachment of solid resulted in a much higher quantity of material becoming immobilized on the electrode surface. For example, the integration of background-corrected slow scan rate cyclic voltammograms in 0.1 M $LiClO_4$ containing 10% CH_3CN indicated that typically between 0.5×10^{-8} and 5.0×10^{-8} mol cm^{-2} of mechanically attached solid was electrolyzed whereas for precipitated layers the values typically ranged from 3.0×10^{-10} to 9.0×10^{-10} mol cm^{-2} and in some cases approached values apparently equivalent to values estimated for monolayer coverage. Both methods produced stable films of adhered solid, although films formed by the physical attachment of the dry solid tended to give rise to broader peaks. The surface precipitation procedure produced a more reproducible voltammetric response.

On immobilization of solid *trans*-$[Mn(CN)(CO)_2\{P(OPh)_3\}(Ph_2PCH_2PPh_2)]$ onto the electrode surface, either by surface precipitation from acetone solution or by mechanical attachment with 0.1 M aqueous $KClO_4$ as the electrolyte, a small but distinct voltammetric response was observed at approximately 0.7 V versus Ag/AgCl, which is close to the value found when the compound was dissolved in acetonitrile. The equation for the solid-state process is summarized in eq 2:

$$[\text{Mn-}\textit{trans}]_{(\text{solid})} + A^-_{(\text{solution})} \rightleftharpoons [\text{Mn-}\textit{trans}^+][A^-]_{(\text{solid})} + e^- \quad (2)$$

The response of electrodes modified in this way was tested in the presence of various electrolyte solutions at concentrations ranging from 0.1 to 2 M as well as with different electrode materials (Au, Pt, glassy carbon, graphite, and paraffin-impregnated graphite).

The solid-state voltammetry was highly dependent on the identity of the electrolyte anion. For example, in the presence of KCl, KF, and $NaNO_3$, no Faradaic current response was detected whereas K_2SO_4 and Na_2SO_4 electrolytes gave rise to responses that were barely distinguishable from the background current. However, with $LiClO_4$, $KClO_4$, KPF_6, and KBF_4 as the electrolytes, a small but distinct wave similar to curve a in Figure 3 was evident. Note that the diminution of the electrochemical response could not be ascribed to problems associated with the stability of the layer being compromised by the presence of aqueous electrolyte, as solid was still clearly visible on the electrode surface after cyclic voltammetric experiments. (See Figure 2.) This unusual anion effect appears to be related to both the size and charge of the ion, with the larger monovalent anions (ClO_4^-, PF_6^-, and BF_4^-) favored over those of smaller ionic radius (F^-, Cl^-, and NO_3^-) and those that are polyvalent (SO_4^{2-}).

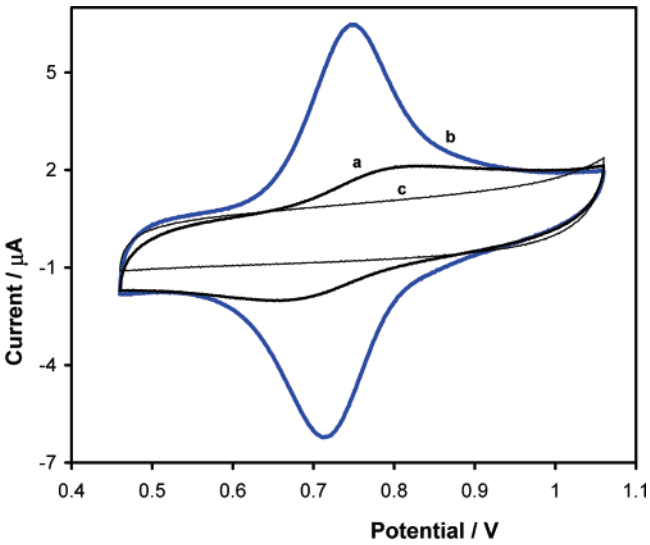

Figure 3. Cyclic voltammograms obtained at a scan rate of 200 mV s^{-1} when a 3-mm glassy carbon electrode is modified with *trans*-$[Mn(CN)(CO)_2\{P(OPh)_3\}(Ph_2PCH_2PPh_2)]$ and then placed in contact with 0.1 M $LiClO_4$ electrolyte containing (a) 0% and (b) 10% acetonitrile. The inner curve (c) shows the background response obtained at a bare electrode (0% acetonitrile).

The magnitude of the faradaic-to-background current ratio did not improve markedly with variations of the electrode material, electrode diameter, layer thickness, electrolyte concentration, or pH or on varying the temperature of the solution between 0 and 40 °C in purely aqueous electrolyte media. However, on adding a small amount of acetonitrile to the electrolyte solution, a marked increase in peak height was observed. This is illustrated in Figure 3, which shows the response of a glassy carbon electrode dip-coated with *trans*-$[Mn(CN)(CO)_2\{P(OPh)_3\}(Ph_2PCH_2PPh_2)]$ in contact with a 0.1 M solution of $LiClO_4$ in H_2O containing 0 and 10% acetonitrile. The background response of the bare electrode is included in the Figure for comparison. The faradaic current in the solution containing 10% acetonitrile is approximately 4 times larger than that for the solvent-free solution and is similar to that expected for a reversible one-electron transfer reaction involving surface-confined species. Specifically, the peak shapes are symmetrical, unlike that expected for a freely diffusing species. Moreover, the peak current scales linearly with scan rate between 0.01 and 2.0 V s^{-1} (for an apparent surface coverage of 3×10^{-10} mol cm^{-2}). This suggests that the response is controlled by finite charge-transport diffusion when the amount of immobilized material is sufficiently small, even at relatively short experimental time scales. However, the peak-to-peak separation between the anodic and cathodic waves, ca. 50 mV at a scan rate of 0.01 V s^{-1}, is greater than the predicted value of 0.00 V for an ideal reversible thin-film model.[25] Also, the peak width at half-height of 125 mV deviates significantly from the theoretical value of 89.1 mV. These nonidealities may be due to ohmic effects, present as a result of uncompensated resistance in the solution or within the layer itself, or to kinetic or thermodynamic dispersion, if the immobilized solid is regarded as a microcrystalline array of particles rather than a thin film.

The variation in signal magnitude between pure aqueous media and media that contained acetonitrile was completely reversible (i.e., when the electrode was transferred from one solution to the other after voltammetric cycling, the voltammetric response characteristic of the new solution was recovered in

TABLE 2: Reversible Potentials for the *trans*^{0}/*trans*$^+$ (Solid) and *cis*^{0}/*cis*$^+$ (Solid) Processes Confined to a Glassy Carbon Electrode Surface in Contact with a 90:10 Mixed Aqueous/Acetonitrile (0.1 M Electrolyte) Medium

	E_{rev}/V[a,b]			
	KPF_6	$KClO_4$	$LiClO_4$	KBF_4[c]
Mn-*trans*	0.68	0.71	0.73	0.78
Mn-*cis*	1.08	1.12	1.14	1.19
anion radius[39]/pm	242	225	225	205
$\Delta_{\beta}^{\alpha}\phi^0$/mV[d]	−7	−83	−83	−121

[a] Potentials quoted relative to Ag/AgCl (3M KCl). [b] Standard deviations ($n = 30$) for E_{rev} (average of E_p^{ox} and E_p^{red}) measurements in the solid state were between 10 and 25 mV. [c] Concentration slightly less than 0.1 M because of limited solubility. [d] Standard anion transfer potential for a mutually saturated water−nitrobenzene system.[32] .

each case). These changes were rapid enough to be apparent on the first voltammetric cycle (at 200 mV s^{-1}) in each experiment.

More complicated behavior was occasionally observed. Specifically, either of the forward or reverse peaks sometimes developed a shoulder with continued cycling of the potential, and oxidation and reduction peaks of differing magnitude were sometimes observed. Although the specific conditions under which this behavior occurred proved difficult to isolate, the effects were more pronounced when the acetonitrile content of the electrolyte solution was increased. One explanation for this may be the formation of a new phase of the immobilized solid, incorporating acetonitrile molecules in its solvation sphere and having a more positive reversible potential (E_{rev}). All other experimental data presented use an acetonitrile content of 10%, as this produced excellent layer stability and a single voltammetric response.

The reversible potential for the complex in the solid state is operationally defined here as the average of the oxidation and reduction peak potentials, with the inherent assumption that the activation overpotentials are the same for both ion insertion and ion expulsion from the layer. These data are summarized in Table 2 and reveal a small dependence on the electrolyte anion radius.When the mechanical attachment mode of immobilization was used, cyclic voltammograms tended to take on characteristics associated with semi-infinite charge-transport diffusion. For example, the peaks showed diffusional tailing, ΔE_p values were >60 mV, and the peak heights scaled linearly with the square root of the scan rate over the low scan-rate range of between 2 and 200 mV s^{-1}. An unusual observation was that after cycling, the magnitude of the faradaic current was frequently seen to increase when the layer was disturbed by, for example, wiping the surface with a tissue. This was presumably a result of more of the attached solid being brought into intimate contact with the electrode surface and suggests that only a small proportion of the solid is electrolyzed, even at long experimental time scales.

To investigate further the effect of acetonitrile, the cyclic voltammetric response of solid *trans*-$[Mn(CN)(CO)_2\{P(OPh)_3\}(Ph_2PCH_2PPh_2)]$, attached by mechanical abrasion, was monitored in solutions containing 0.1 M $KClO_4$, where the acetonitrile content was increased from 0 to 44%. Figure 4 shows the variation in peak height (I_p, top curve) and the number of moles per cm^2 that were oxidized and reduced (Γ, bottom curve) for a scan rate of 200 mV s^{-1}. The electrode was allowed to equilibrate for 3 min prior to commencing each experiment, and the 10th cycle in each CV experiment was used to obtain the data. As can be seen from Figure 4, the effect of acetonitrile is quite dramatic, with peak currents increasing from less than

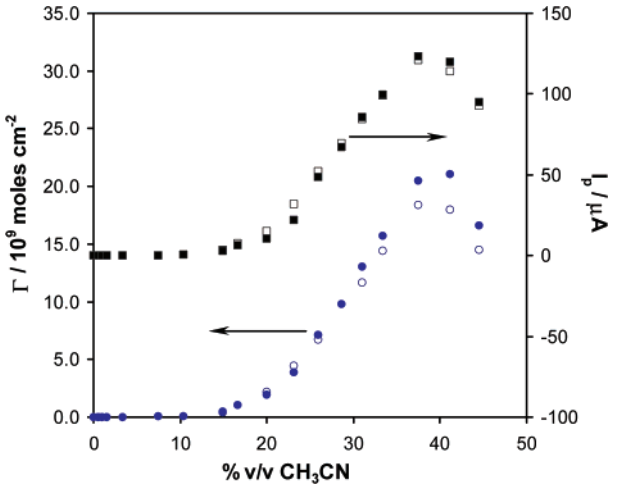

Figure 4. Dependence of the peak heights ($I_{p,red}$, ■; $I_{p,ox}$, □) and moles per cm^2 of oxidized and reduced solid (Γ_{red}, ●; Γ_{ox}, ○) on acetonitrile content when acetonitrile/water (0.1 M $LiClO_4$) electrolyte is used for the oxidation of *trans*-$[Mn(CN)(CO)_2\{P(OPh)_3\}(Ph_2PCH_2PPh_2)]$ adhered to a glassy carbon electrode. The scan rate is 200 mV s^{-1}.

SCHEME 1: Square Scheme for Redox-Induced *cis*/*trans* Isomerization

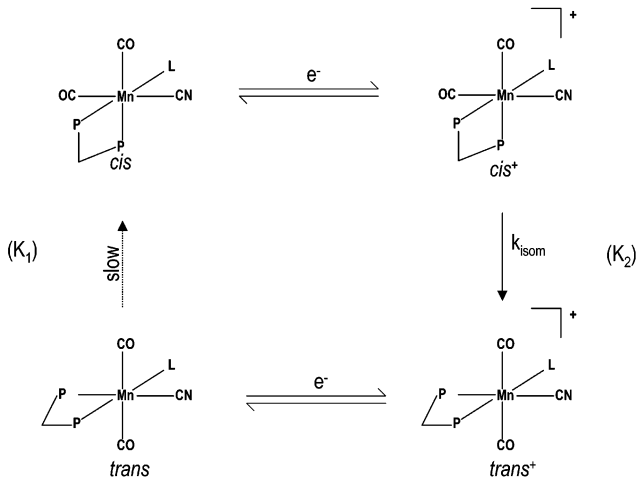

0.5 μA to greater than 120 μA as the percentage of acetonitrile is increased from 0 to 38%, and the amount of material that is electroactive on the electrode surface at this scan rate increases from 2×10^{-11} to ca. 2×10^{-8} moles cm^{-2} in the same range. These results suggest that a far greater proportion of the attached solid is electrolyzed when acetonitrile is present in the contacting electrolyte solution, though only in the presence of certain anions as discussed above. We believe that this behavior is due to the reversible incorporation of solvent into the solid lattice, facilitating a greater flux of charge-compensating ions across the solid−liquid interface.

The response of the system begins to diminish at higher acetonitrile levels, and by 45%, the voltammetry is characterized by a rapid decrease in signal with each potential cycle. If at this stage the electrode is transferred to a solution containing 10% acetonitrile, then the peak height does not recover its original value. This indicates that the oxidized *trans*$^+$ cation is soluble on the voltammetric time scale when a high concentration of acetonitrile is present. Other organic solvents (dimethylformamide and tetrahydrofuran) showed a similar effect to acetonitrile in enhancing the voltammetric response.

***cis*-$[Mn(CN)(CO)_2\{P(OPh)_3\}(Ph_2PCH_2PPh_2)]$. Solution-Phase Electrochemistry.** The cyclic voltammetric behavior of

a 3.0 mM solution of Mn-*cis* dissolved in acetonitrile (0.1 M $[Bu_4N][PF_6]$) at a 3-mm-diameter glassy carbon electrode is illustrated in Figure 1b. In the initial positive potential direction scan, there are no peaks observed until a potential of ca. 1.17 V is reached, where a totally irreversible (scan rate of 200 mV s^{-1}) process is observed, corresponding to the oxidation of the 18-electron Mn-*cis* complex. In the reverse scan and in subsequent cycles, a new reversible redox couple is evident, with $E_f{}^0 = 0.72$ V, which is identical to the value previously observed for the Mn-*trans*/Mn-*trans*$^+$ couple. Thus, the cyclic voltammetric behavior for the oxidation of Mn-*cis* can be characterized as an $\vec{E}\vec{C}\vec{E}\vec{C}$ process, as shown in Scheme 1, with the first chemical step corresponding to the isomerization of the thermodynamically unstable 17-electron *cis*$^+$ complex. Reconversion of *trans*^{0} to the *cis*^{0} form occurs only at a very slow rate and is not observed on the time scale of these experiments; infrared measurements made at intervals on a deoxygenated and sealed solution of the *trans* isomer dissolved in dichloromethane indicated that the reconversion reaction had not reached equilibrium after 350 h. The ratio of the equilibrium constants for the two processes is given by the following equation:[26]

$$\frac{K_2}{K_1} = \exp\left[\frac{F}{RT}\{E_f{}^0(cis^{0/+}) - E_f{}^0(trans^{0/+})\}\right] \qquad (3)$$

where K_2 is the equilibrium constant for the conversion of *cis*$^+$ to *trans*$^+$ and K_1 is the equilibrium constant for the conversion of *trans*^{0} to *cis*^{0}; see Scheme 1. On the basis of the data in Table 1, (K_2/K_1) is in excess of 10^7 when acetonitrile is used as the solvent. Qualitatively similar voltammetric behavior was observed for these compounds in dichloromethane, but with potentials shifted to slightly more negative values; see Table 1.

At sufficiently short cyclic voltammetric experimental time scales (e.g., scan rate ≥ 100 V s^{-1}), the isomerization step could be outrun so that no *trans*$^{0/+}$ couple was observed on cycling the potential. That is, only peaks corresponding to the oxidation and reduction of the Mn-*cis* complex were observed; under this condition, the process simplifies to

$$\text{Mn-}cis_{(\text{solution})} \rightleftharpoons \text{Mn-}cis^+{}_{(\text{solution})} + e^- \qquad (4)$$

Evaluation of Kinetic Parameters. As shown in Figure 5, a cyclic voltammogram recorded at a scan rate of 4.96 V s^{-1} agrees very well with digital simulation results when k_{isom}[27] is set at 38 s^{-1}. In these experiments, a Pt microelectrode was used to minimize the influence of uncompensated resistance. The heterogeneous rate constant was determined to be 0.06 ± 0.01 cm s^{-1} using eq 1, as described for the Mn-*trans* species. Scan rates above 50 V s^{-1} were used to obtain the value of $k°$ to isolate the heterogeneous charge transfer from the homogeneous kinetics. Similar agreement between experiment and simulation was obtained for scan rates up to 400 V s^{-1}, and the same kinetic parameters fitted the data without significant error when the concentration was varied over the range of 0.5 to 5 mM and when dichloromethane was used as the solvent instead of acetonitrile.

Figure 6 shows the dependence of the cyclic voltammetric response on scan rate. The current (*y* axis) of this graph has been divided by $\nu^{1/2}$ to normalize approximately for linear diffusion mass transport rates so that the differences between curves at various scan rates become primarily due to the contribution from homogeneous kinetics. (The contribution to the total current from hemispherical diffusion has been neglected in the normalization). As can be seen in Figure 6, at a scan rate

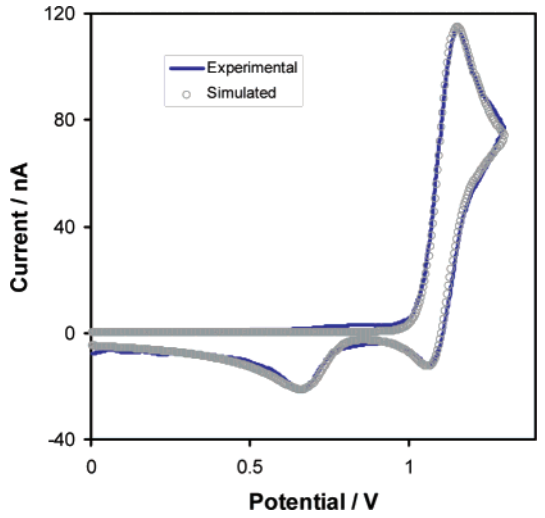

Figure 5. Comparison of experimental and simulated cyclic voltammograms for the oxidation of 3.1 mM *cis*-$[Mn(CN)(CO)_2\{P(OPh)_3\}(Ph_2PCH_2PPh_2)]$ in acetonitrile (0.1 M $[Bu_4N][PF_6]$) at a Pt microelectrode. The scan rate was 4.96 V s^{-1}. Simulation parameters are electrode radius = 1.77×10^{-3} cm, $E^0_{f1} = 1.17$ V, $E^0_{f2} = 0.72$ V, concentration = 3.2 mM, $D_1 = D_2 = 7.2 \times 10^{-6}$ cm s^{-1}, $K_{eq} = 28$, $k° = 0.06$ cm s^{-1}, and $\alpha = 0.5$.

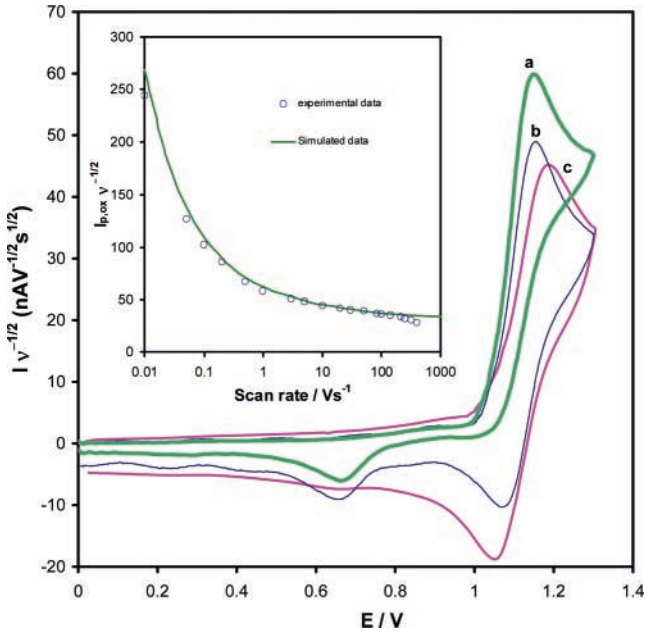

Figure 6. Cyclic voltammograms obtained at scan rates of (a) 1.0, (b) 9.9, and (c) 97.8 V s^{-1} for the oxidation of *cis*-$[Mn(CN)(CO)_2\{P(OPh)_3\}(Ph_2PCH_2PPh_2)]$ at a 25-μm-diameter Pt microelectrode. The inset shows the variation of peak current with scan rate. The *y* axis has been normalized by a factor of $\nu^{-1/2}$ for all plots to minimize the differences in mass transport rates. Other conditions and simulation parameters are the same as for Figure 5.

of 1 V s^{-1}, the process corresponding to the oxidation of *cis*-$[Mn(CN)(CO)_2\{P(OPh)_3\}(Ph_2PCH_2PPh_2)]$ is totally irreversible. On increasing the scan rate, a reduction component at 1.17 V, consistent with the reduction of *cis*$^+$, starts to appear. Finally, when a scan rate of 100 V s^{-1} is used, the oxidation of *cis*-$[Mn(CN)(CO)_2\{P(OPh)_3\}(Ph_2PCH_2PPh_2)]$ is fully reversible, with the reduction process due to the product, *trans*-$[Mn(CN)(CO)_2\{P(OPh)_3\}(Ph_2PCH_2PPh_2)]^+$, absent or negligible.

The inset to Figure 6 shows the experimental and theoretical dependence of the response on the scan rate for the oxidation of *cis*-$[Mn(CN)(CO)_2\{P(OPh)_3\}(Ph_2PCH_2PPh_2)]$. The theory

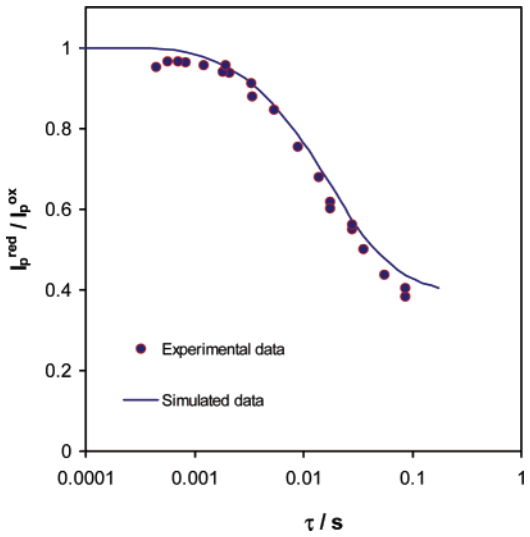

Figure 7. Dependence on the experimental time scale τ, where $\tau = (E_\lambda - E^0_f)/\nu$, of the ratio of reduction and oxidation peak currents obtained under conditions of cyclic voltammetry at a 25-μm Pt microelectrode for the oxidation of *cis*-[Mn(CN)(CO)$_2${P(OPh)$_3$}(Ph$_2$PCH$_2$PPh$_2$)] in acetonitrile (0.1 M [Bu$_4$][NPF$_6$]). The solid line represents data simulated using the same parameters as in Figure 5.

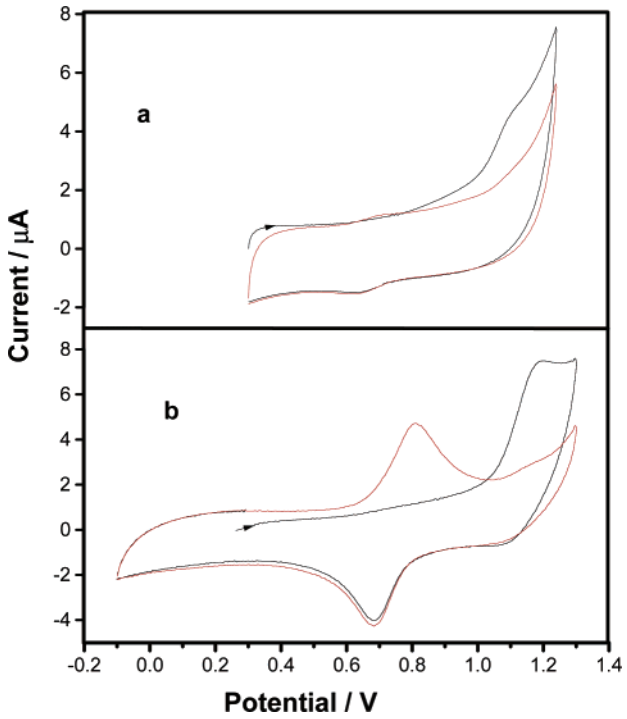

Figure 8. Solid-state voltammograms at a scan rate of 0.2 V s^{-1} for the oxidation of *cis*-[Mn(CN)(CO)$_2${P(OPh)$_3$}(Ph$_2$PCH$_2$PPh$_2$)] mechanically attached to a 3-mm glassy carbon electrode in contact with an aqueous solution containing (a) aqueous 0.1 M LiClO$_4$ and (b) aqueous 0.1 M LiClO$_4$ containing 10% acetonitrile.

was modeled using digital simulation (hemispherical approximation) and compared to the experimental data in the scan-rate range from 0.01 V s^{-1} to approximately 400 V s^{-1}. The graph does not plateau at low scan rates, as would be the case for a purely linear diffusion regime, but continues to increase as a result of the spherical nature of the diffusion field. In the simulation, a value of 38 s^{-1} was used for the homogeneous rate constant (k_{isom}), and values of 0.06 and 0.065 cm s^{-1} were used for the heterogeneous rate constants ($k°$) for the *cis* and *trans* processes, respectively. Excellent agreement between experimental and simulated data is found over the scan-rate range of 3 to 143 V s^{-1}. The small deviation at very high scan rates above ca. 150 V s^{-1} may be due to increasing uncertainty in defining the baseline as the scan rate is increased. Below scan rates of 1 V s^{-1}, the deviation from predicted values becomes more significant as the time scale of the experiment is increased. This deviation is attributed to the use of the hemispherical approximation under conditions where chemical control is significant. While acknowledging the limitations of treating voltammetry at microdisk electrodes by approximation to a 1D (hemispherical) diffusion problem,[28] we regard the use of this approximation, particularly at the higher scan rates, as being of sufficient accuracy for our purposes.

To confirm the value of k_{isom} and as a test of the internal consistency of the data analysis, the ratio (I_p^{red}/I_p^{ox}) of peak currents for the oxidation and reduction components associated with the *cis*-[Mn(CN)(CO)$_2${P(OPh)$_3$}(Ph$_2$PCH$_2$PPh$_2$)] species was also analyzed as a function of scan rate. This is a useful strategy since the ratio is independent of electrode area, diffusion coefficient, and concentration of reactant for a first-order process. Thus, a precise knowledge of these values is not required.

Figure 7 shows the variation of the ratio of peak heights with the parameter τ, the time taken from E_f to the switching potential E_λ. In this case, it is necessary to normalize the data using τ instead of the scan rate because the magnitude of the return peak is a function of E_λ.[29] In these experiments, different values of E_λ were used at each scan rate to ensure the reliability of the experimental data. As expected, the ratio of peak heights continues to increase with a decreasing experimental time scale until reversible behavior is observed at very short time scales and the current ratio plateaus at unity. The data are compared to the theoretical curve expected for a charge-transfer oxidation process followed by a chemical reaction with a homogeneous rate constant of 38 s^{-1}. Again, generally excellent agreement is found between experiment and theory. The small deviation at slow scan rates arises because of the difficulty of measuring the smallest of the reduction peaks whereas the small deviations at the highest scan rates are associated with uncertainty in determining the position of the baseline. The quantitative data obtained in this study are consistent with the initial qualitative voltammetric studies.[22]

Solid-State Electrochemistry. The immobilization of solid *cis*-[Mn(CN)(CO)$_2${P(OPh)$_3$}(Ph$_2$PCH$_2$PPh$_2$)], either by surface precipitation from acetone solution or by mechanical abrasion of the solid onto an electrode surface and then placing the electrode in contact with aqueous electrolyte solution, gives rise to voltammetry that parallels some aspects of that of the *trans* species. For example, electrolysis is far more efficient in electrolyte solutions containing ClO_4^-, PF_6^-, or BF_4^- anions, and the response is markedly enhanced by the presence of small amounts of acetonitrile.

Figure 8a and b shows the response at a glassy carbon electrode with mechanically attached Mn-*cis*, in contact with an aqueous 0.1 M solution of LiClO$_4$, that contained 0 and 10% acetonitrile, respectively. As was the case with the immobilized *trans* species, the magnitude of the response is significantly enhanced in the presence of the organic solvent. Similar to the solution-phase studies, the only peak observed on the first forward scan is that corresponding to the oxidation of the *cis* species (E_{rev}= 1.135 V vs Ag/AgCl). In subsequent cycles of the potential, this peak either disappears or steadily decreases in magnitude (depending on the amount of immobilized solid), and a new redox couple with the same reversible potential as

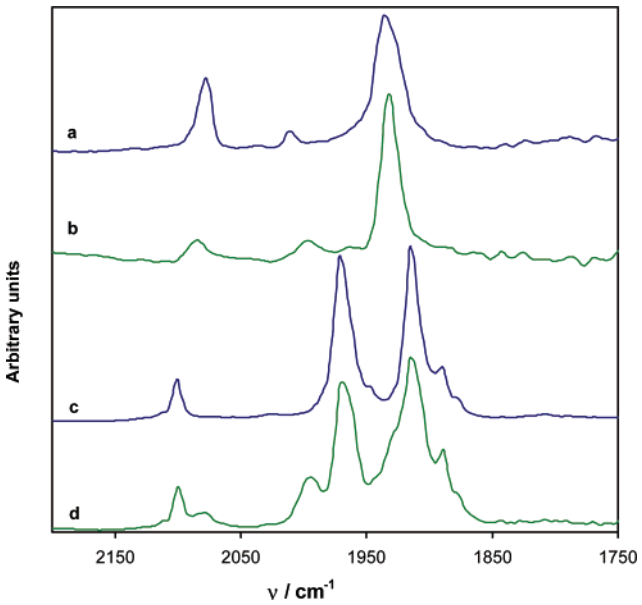

Figure 9. Infrared spectra of immobilized solid (a) *trans*- and (c) *cis*-[Mn(CN)(CO)$_2${P(OPh)$_3$}(Ph$_2$PCH$_2$PPh$_2$)] prior to electrolysis. Spectrum b is of the *trans* complex and spectrum d of the *cis* complex after potential cycling at a scan rate of 0.2 V s^{-1} and electrolysis at 1.25 V vs Ag/AgCl for 10 min in 0.1 M KPF_6 containing 15% acetonitrile.

the immobilized *trans* form ($E^0_f = 0.73$ V) becomes evident. The equation for the solid-state process can be summarized as follows:

$$[\text{Mn-}cis]_{(\text{solid})} + \text{A}^-_{\ (\text{solution})} \rightleftharpoons [\text{Mn-}cis^+][\text{A}^-]_{(\text{solid})} + \text{e}^- \quad (5)$$

$$[\text{Mn-}cis^+][\text{A}^-]_{(\text{solid})} \xrightarrow{k_{\text{isom}}} [\text{Mn-}trans^+][\text{A}^-]_{(\text{solid})} \quad (6)$$

$$[\text{Mn-}trans^+][\text{A}^-]_{(\text{solid})} + \text{e}^- \rightleftharpoons [\text{Mn-}trans\ ]_{(\text{solid})} + \text{A}^-_{\ (\text{solution})} \quad (7)$$

Other voltammetric features associated with immobilized layers of *cis*-[Mn(CN)(CO)$_2${P(OPh)$_3$}(Ph$_2$PCH$_2$PPh$_2$)], following isomerization, are identical to those associated with immobilized *trans*-[Mn(CN)(CO)$_2${P(OPh)$_3$}(Ph$_2$PCH$_2$PPh$_2$)]. For example, the transition from finite to semi-infinite diffusional behavior as the scan rate or the layer thickness is increased is also observed under these conditions. However, it was evident that the observation of the reversibility of the cis^0/cis^+ process could be achieved at far lower scan rates than was the case in the solution phase.

The isomerization reaction in the solid state was probed using diffuse reflectance infrared spectrometry. Figure 9 shows infrared spectra obtained for layers of both the *cis* and *trans* complexes immobilized on a glassy carbon electrode before and after electrolysis. The infrared spectrum of the *trans* species before electrolysis (a) shows one strong band for carbonyl at 1934 cm^{-1} plus a weak band for the forbidden A mode at 2010 cm^{-1}, with the cyanide ligand band being detectable at 2077 cm^{-1}. The pre-electrolysis immobilized *cis* form (c) has two strong bands at 1971 and 1913 cm^{-1} for the carbonyl and a weak band at 2100 cm^{-1} for the cyanide. The positions and relative intensities of these bands are all similar to those observed for the compounds dissolved in dichloromethane.[22,30]

Spectra b and d in Figure 9 show the infrared response for the *trans* and *cis* species immobilized on glassy carbon after cycling the potential at a scan rate of 200 mV s^{-1} between 0.2 and 1.25 V, followed by electrolysis at 1.25 V for 10 min in a 0.1 M solution of KPF_6 that contained 15% acetonitrile. Infrared spectrum b shows the emergence of a peak situated at 1992 cm^{-1} as the immobilized solid is oxidized to the $trans^+$ species in accordance with eq 3 above. The location of this $trans^+$ band is similar to the value obtained in the solution phase for the *trans* cation.[22] In spectrum d, the electrochemically induced isomerization is clearly evidenced by the fact that peaks characteristic of the *cis*, *trans*, and $trans^+$ species are now observed. The cyanide peaks for both *cis* and *trans* are clearly identifiable around 2100 cm^{-1}, the two carbonyl bands for the *trans* neutral species are partially hidden but are easily discerned in the second-derivative spectrum, and the carbonyl stretching frequency for the $trans^+$ cation also appears at the same frequency as in spectrum b. No change in the infrared spectrum of the immobilized *cis* complex was observed on cycling the potential or on electrolysis unless at least 15% acetonitrile was present in the contacting electrolyte solution. Also, it was required that the amount of immobilized solid be relatively small in order to observe the spectral changes associated with the *cis*−*trans* isomerization. Significantly, even after the complete disappearance of the peak in the cyclic voltammetric experiment, corresponding to the oxidation of the *cis* complex, which typically happened within the first three to four cycles, the bands characteristic of this species were often still predominant in the infrared spectrum. These observations suggest that, even when electrolysis is carried out for long periods of time (>15 min), significant portions of the solid remain electrochemically isolated from the electrode and are consistent with ion insertion into the solid matrix occurring at the electrode/solid/solution triple interface, as expected for a nucleation and growth type mechanism. Our earlier observation of increased Faradaic current after the physical external disturbance of the layer also supports this view.

To estimate the influence of isomerization in the solid-state voltammograms relative to those obtained in solution-phase studies, the voltammetry was theoretically simulated as a thin-layer problem. This approach is substantiated by our observation of finite diffusional type behavior over a wide range of scan rates when surface precipitation is used to immobilize the solid and the voltammetry is conducted in the presence of mixed aqueous/organic solution. An analogous oxidation-to-reduction peak-current ratio method of data analysis to that used for the solution-phase studies was employed; it was reasoned that this method would show the greatest immunity to parameters such as layer thickness and the mass and distribution of the solid, which are difficult to control in the solid-state experiment. Therefore, cyclic voltammetric experiments were carried out on freshly dip-coated layers in aqueous 0.1 M $KClO_4$ electrolyte media containing 10% acetonitrile at scan rates ranging from 0.05 to 20 V s^{-1} and, as with the solution phase studies, varying switching potentials (E_λ) were again used. The ratio of the reduction peak current to that for the oxidation was then plotted as a function of τ, the time from E_{rev} to E_λ. Figure 10 shows a pattern similar to that for the solution phase, with the ratio of peak heights increasing with scan rate (smaller τ) until full reversibility is reached and the ratio plateaus at unity. The most important difference between these data and those in Figure 7 is that the position of the curve is shifted to longer experimental time scales by approximately 230 ms, indicating a significantly slower rate of isomerization than that obtained in purely solution-phase studies. By analyzing the position of the peak in the first differential of the curve in Figure 10, the rate of isomerization in the solid is estimated at 2.0 s^{-1}. The solid line

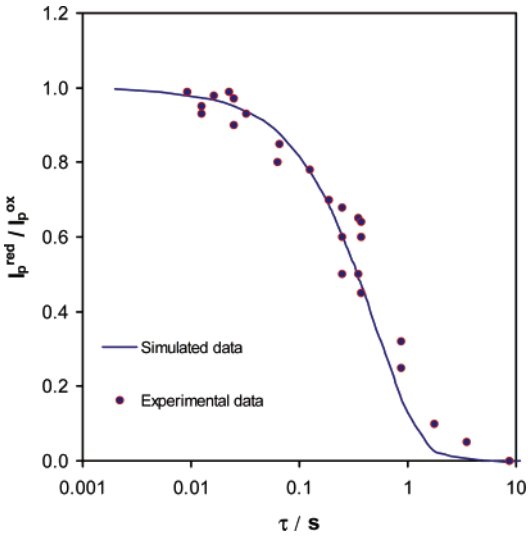

Figure 10. Dependence on the experimental time scale τ of the ratio of the reduction and oxidation peak currents for solid *cis*-[Mn(CN)(CO)$_2${P(OPh)$_3$}(Ph$_2$PCH$_2$PPh$_2$)] immobilized on a 3-mm glassy carbon electrode. Contacting solution is 90:10 H_2O/acetonitrile (0.1 M $KClO_4$) electrolyte media. The solid line is the theoretical relationship calculated using a thin-layer model with an isomerization rate (k_{isom}) of 2 s^{-1}.

in Figure 10 shows the result of digital simulations using the finite diffusional model. Good agreement is observed with the isomerization rate constant set to 2.0 s^{-1}.

Conclusions

Solution-phase voltammetric studies of *cis*- and *trans*-[Mn(CN)(CO)$_2${P(OPh)$_3$}(Ph$_2$PCH$_2$PPh$_2$)] in acetonitrile have shown that the *trans*^{0}/*trans*$^+$ process has a formal potential (E^0_f) of 0.72 V in CH_3CN. The oxidation of the *cis* species gives rise to an *E*C*E*C mechanism in which the *trans*$^+$ product is reduced at a potential more negative than the formal potential of the *cis*/*cis*$^+$ couple, which has a value of 1.170 V in CH_3CN. The rate of the *cis*$^+$ → *trans*$^+$ isomerization process, as measured using fast-scan cyclic voltammetry with comparison to digital simulation, is 38 s^{-1}; the reconversion reaction (*trans*^{0} → *cis*^{0}) does not occur on the time scale of a cyclic voltammetric experiment. The heterogeneous rate constants at a platinum microelectrode were measured to be 0.06 and 0.065 cm s^{-1} for the *cis*^{0}/*cis*$^+$ and *trans*^{0}/*trans*$^+$ couples, respectively. The behavior of both isomers in dichloromethane is qualitatively similar but with the formal potentials occurring at slightly less positive potentials.

When *cis*- or *trans*-[Mn(CN)(CO)$_2${P(OPh)$_3$}(dppm)] is attached to an electrode surface as a solid layer, either by mechanical attachment or by the surface precipitation procedure, small faradaic currents are detected in the presence of aqueous $LiClO_4$, $KClO_4$, KPF_6, and KBF_4 electrolyte media, but no detectable electrolysis is evident when KCl, KF, KNO_3, K_2SO_4, or Na_2SO_4 is used as the supporting electrolyte. The addition of acetonitrile to the aqueous solution dramatically increases the magnitude of the peak currents observed under conditions of cyclic voltammetry for the first four mentioned electrolytes, but voltammetric silence is retained when any of the other electrolytes are used. Other organic solvents (dimethylformamide, tetrahydrofuran) are found to enhance the voltammetric response in an analogous manner. On cycling the potential, electron scanning micrographs reveal needle-shaped microcrystals in a morphology that presumably enables the rapid transport of ClO_4^-, PF_6^-, and BF_4^- into and out of the solid.

The fact that the effect of organic solvent is reversible indicates that the signal enhancement may be related to the reversible incorporation of solvent into the lattice, thereby facilitating the rate of the charge-neutralization process, which involves the transport of the anion from the solution to the solid phase.

The effect of anionic charge and radius, with the larger monovalent anions (ClO_4^-, PF_6^-, and BF_4^-) giving rise to a greater faradaic response than those of smaller ionic radius (F^-, Cl^-, and NO_3^-) and those that are polyvalent (SO_4^{2-}), can be understood as an effect of the surface charge density of these species. Anions of low charge density will tend to be weakly solvated[31] and thus more hydrophobic, allowing more facile transport across the solution−solid interface through ion channels formed by the organic ligands. The data in Table 2 support this view, with the reversible potentials for the immobilized *trans* complex in the presence of each anion increasing with decreasing ionic radius. As shown in Table 2, an interesting correlation also exists for the energy of partitioning the anions at an oil−water interface; it may also be noted that the anions NO_3^-, Cl^-, and F^-, which did not give rise to any electrochemical response for the attached solid, all have transfer potentials that are considerably more negative (−253, −316, and −454 mV, respectively).[32] These observations suggest that the free energy of transfer of the charge-compensating ions from solution into the solid phase is an important term in the electrochemical response of these systems.

We note that the observed dependence is similar to the Hofmeister series of anions, for example,

$$ClO_4^- > SCN^- > NO_3^- > Cl^- > F^- > SO_4^{2-}$$

that represents their lipophilicity.[33] The series originates from the ranking of various ions regarding their ability to stabilize the structure of proteins but has been invoked in discussions of, for example, salt effects on the Diels−Alder reaction[34] and proton acceptor abilities of anions.[31] We reason that ions that rank highly in this series are allowed facile ingress and egress to the immobilized solid during electrolysis/charge neutralization (eqs 2, 5, and 7) whereas those that rank lowly are effectively excluded. Similar instances have been reported previously; for example, ion-selective electrodes based on quaternary ammonium or phosphonium salts usually display anion selectivity corresponding to the Hofmeister series,[35,36] and ion insertion rates into electropolymerized films such as polypyrrole[37] and polyaniline[38] have been shown to follow a similar order. We also note that the incorporation of organic solvent into the solid lattice may have the effect of assisting the transport of the more hydrophobic ions through the solid, facilitating deeper penetration and giving rise to higher Faradaic currents.

Infrared measurements conducted on the solid immobilized on glassy carbon before and after electrolysis clearly demonstrate the occurrence of the *cis*−*trans* isomerization in the solid state. It is also apparent from these measurements and from other observations that even under conditions that should ensure exhaustive oxidation a significant fraction of the immobilized material, which is not in intimate contact with the electrode, does not undergo conversion and remains electrochemically isolated from the remainder of the attached solid.

The rate of isomerization of *cis*-[Mn(CN)(CO)$_2${P(OPh)$_3$}(Ph$_2$PCH$_2$PPh$_2$)] in the solid state was calculated by probing the ratio of oxidation and reduction peak heights as a function of scan rate. Comparison with digitally simulated responses indicated an isomerization rate of 2.0 s^{-1}, which is significantly slower than the solution-phase rate of 38 s^{-1}. This can be readily

understood if the restriction of free space for isomeric change in the solid-state matrix relative to the solution-phase situation is considered. The solvent independence of the isomerization rate in the solution phase and the fact that it occurs at an observable rate in the solid state suggest that the conformational change proceeds via a twist mechanism rather than through a dissociative (metal−ligand bond-breaking) process.

Acknowledgment. Extensive discussions with Dr. Jie Zhang (Monash University) and financial support from the Australian Research Council are gratefully acknowledged.

References and Notes

(1) Liu, Z. F.; Hashimoto, K.; Fujishima, A. *Nature (London)* **1990**, *347*, 658.

(2) Liu, Z. F.; Morigaki, K.; Hashimoto, F.; Fujishima, A. *Anal. Chem.* **1992**, *64*, 134.

(3) Hapiot, P.; Neudeck, A.; Pinson, J.; Novi, M.; Petrillo, G.; Tavani, C. *J. Electroanal. Chem.* **1997**, *422*, 99.

(4) Tahibana, H.; Nakamura, M.; Matsumoto, H.; Komizu, H.; Manda, E.; Niino, H.; Yabe, A.; Kawabata, Y. *J. Am. Chem. Soc.* **1989**, *111*, 3080.

(5) Armaroli, N.; Balzani, V.; Collin, J.; Gavini, P.; Sauvage, J.; Ventura, B. *J. Am. Chem. Soc.* **1999**, *121*, 4397.

(6) Pascher, T.; Chesick, J. P.; Winkler, J. R.; Gray, H. B. *Science (Washington, D.C.)* **1996**, *271*, 1558.

(7) Stoll, M. E.; Belazoni, P.; Calhorda, M. J.; Drew, M. G. B.; Felix, V.; Geiger, C. A.; Gamelas, C. A.; Concalves, I. S.; Romao, C. C.; Veiros, L. F. *J. Am. Chem. Soc.* **2001**, *123*, 10595.

(8) Bond, A. M.; Carr, S. W.; Colton, R. *Organometallics* **1984**, *3*, 541.

(9) Bond, A. M.; Grabaric, B. S.; Grabaric, Z. *Inorg. Chem.* **1978**, *17*, 1013.

(10) Bond, A. M.; Grabaric, B. S.; Jackowaki, J. J. *Inorg. Chem.* **1978**, *17*, 2153.

(11) Vallat, A.; Person, M.; Roullier, L.; Laviron, E. *Inorg. Chem.* **1987**, *26*, 332.

(12) Zawisza, I.; Bilewicz, R.; Luboch, E.; Biernat, J. F *J. Electroanal. Chem.* **1999**, *471*, 156.

(13) Batz, V.; Schneeweiss, M. A.; Kramer, D.; Hagensrom, H.; Kolb, D. M.; Mandler, D. *J. Electroanal. Chem.* **2000**, *491*, 55.

(14) Wang, Y. Q.; Yu, H. Z.; Mu, T.; Luo, Y.; Zhao, C. X.; Liue, Z. F. *J. Electroanal. Chem.* **1997**, *438*, 127.

(15) Bond, A. M.; Sholtz, F. *Langmuir* **1991**, *7*, 3197.

(16) Keane, L.; Hogan, C. F.; Forster, R. J. *Langmuir* **2002**, *18*, 4826.

(17) Bond, A. M.; Colton, R.; Marken, F.; Walter, J. N. *Organometallics* **1994**, *13*, 5122.

(18) Dostal, A.; Schroder, U. Scholz, F. *Inorg. Chem.* **1995**, *34*, 1711.

(19) Dostal, A.; Meyer, B.; Scholz, F.; Schroder, U.; Bond, A. M.; Marken, F.; Shaw, S. J. *J. Phys. Chem.* **1995**, *99*, 2096.

(20) Carriedo, G. A.; Riera, V.; Connelly, N. G.; Raven, S. J. *J. Chem. Soc., Dalton Trans.* **1987**, 1769.

(21) Connelly, N. G.; Geiger, W. E. *Chem. Rev.* **1996**, *96*, 877.

(22) Connelly, N. G.; Hassard, K. A.; Dunne, B. J.; Orpen, A. G.; Raven, S. J.; Carriedo, G. A.; Riera, V. *J. Chem. Soc., Dalton Trans.* **1988**, 1623.

(23) Bombin, F.; Carriedo, G. A.; Miguel, J. A.; Riera, V. *J. Chem. Soc., Dalton Trans.* **1981**, 2049.

(24) Nicholson, R. S. *Anal. Chem.* **1965**, *37*, 1351.

(25) Bard, A. J.; Faulkner, L. R. *Electrochemical Methods: Fundamentals and Applications*, 2nd ed.; Wiley: NewYork, 2001; Chapter 14, p 591.

(26) Pombeiro, A. J. L.; Guedes da Silva, M. F. C.; Lemos, M. A. N. D. A. *Coord. Chem. Rev.* **2001**, *219*−*221*, 53.

(27) Other parameters used: hemisphere radius = 1.77×10^{-3} cm, $E_1 = 1.168$ V, $E_2 = 0.723$ V, concentration = 3.2 mM, $D_1 = D_2 = 7.2 \times 10^{-6}$ cm s^{-1}, $K_{eq} = 28$, $k^0 = 0.06$ cm s^{-1}, $\alpha = 0.5$.

(28) Alden, J. A.; Hutchinson, F.; Compton, R. G. *J. Phys. Chem. B* **1997**, *101*, 949.

(29) Nicholson, R. S.; Shain, I. *Anal. Chem.* **1965**, *37*, 190.

(30) Carriedo, G. A.; Crespo, M. C.; Riera, V.; Sanchez, M. G.; Valin, M. L.; Moreiras D.; Solans, X. *J. Organomet. Chem.* **1986**, *302*, 47.

(31) Taylor, R. P.; Kuntz, I. D., Jr. *J. Am. Chem. Soc.* **1972**, *94*, 7963.

(32) Vuolkov, A. G.; Deamer, D. W.; Tanelian, D. L.; Markin, V. S. *Liquid Interfaces in Chemistry and Biology*; Wiley: NewYork, 1998; p 134.

(33) Sollner, K.; Shean, G. M. *J. Am. Chem. Soc.* **1964**, *86*, 1901.

(34) Rizzo, C. J. *J. Org. Chem.* **1992**, *57*, 6382.

(35) Wang, J. *Analytical Electrochemistry*; Wiley: NewYork, 1994; Chapter 4, p 119.

(36) Sjoberg, P.; Bobaka, J.; Lewenstam, A.; Ivaska, A. *Electroanalysis* **1999**, *11*, 821.

(37) Tamm, J.; Alumma, A.; Hallik, A.; Silk, T. Sammelselg, V. *J. Electroanal. Chem.* **1996**, *414*, 149.

(38) Choi, S. J.; Park, S. M. *J. Electrochem. Soc.* **2002**, *149*, E26.

(39) Roobottom, H. K. http://www.warwick.ac.uk/fac/sci/Chemistry/thermochemistry/ thermo7b.htm, September 14, 2002.